Electronic Supplementary Material (ESI) for Sustainable Energy & Fuels.

Electronic Supporting Information

Revealing the role of Rh valence state, La doping level and Ru cocatalyst in determining the H_2 evolution efficiency in doped $SrTiO_3$ photocatalysts

Dharmapura H. K. Murthy[a], Hiroyuki Matsuzaki[a], Qian Wang[b,c], Yohichi Suzuki[a], Kazuhiko Seki[a], Takashi Hisatomi[b,c #], Taro Yamada[b,c], Akihiko Kudo[d], Kazunari Domen[b,c #] and Akihiro Furube[a,e]

a. National Institute of Advanced Industrial Science and Technology (AIST), Tsukuba Central 2, 1-1-1 Umezono, Tsukuba, Ibaraki 305-8568, Japan.

b. Department of Chemical System Engineering, School of Engineering, The University of Tokyo, 7-3-1 Hongo, Bunkyo-ku, Tokyo 113-8656, Japan.

c. Japan Technological Research Association of Artificial Photosynthetic Chemical Process (ARPChem), 2-11-9 Iwamotocho, Chiyoda-ku, Tokyo 101-0032, Japan

d. Department of Applied Chemistry, Faculty of Science, Science University of Tokyo, 1-3 Kagurazaka, Shinjuku-ku, Tokyo 162-8601, Japan.

e. Department of Optical Science, Tokushima University, 2-1 Minamijosanjima-cho,
Tokushima 770-8506, Japan.

\# Current affiliation: Centre for Energy & Environmental Science, Shinshu University, 4-17-1 Wakasato, Nagano-shi, Nagano 380-8553, Japan.

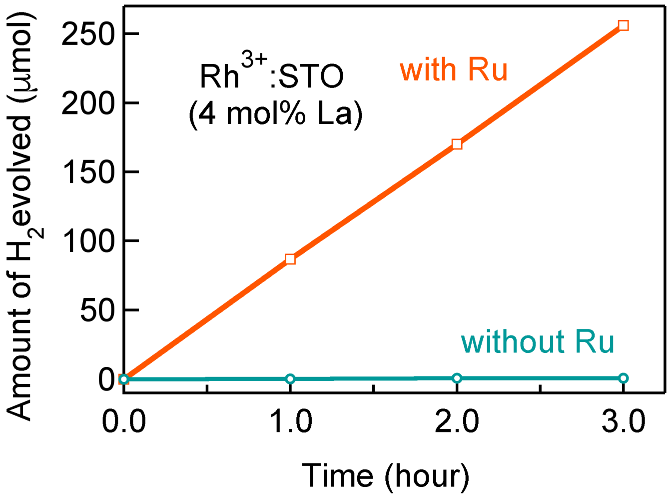

Figure S1. Amount of H_2 evolved during the photocatalytic reaction for Rh^{3+}: STO (4 mol% La) with and without the ruthenium (Ru) cocatalyst loading. Reaction conditions: catalyst, 0.3 g; reactant solution, 150 mL of 10 vol.% aqueous methanol solution; light source, 300 W xenon lamp (λ > 420 nm).

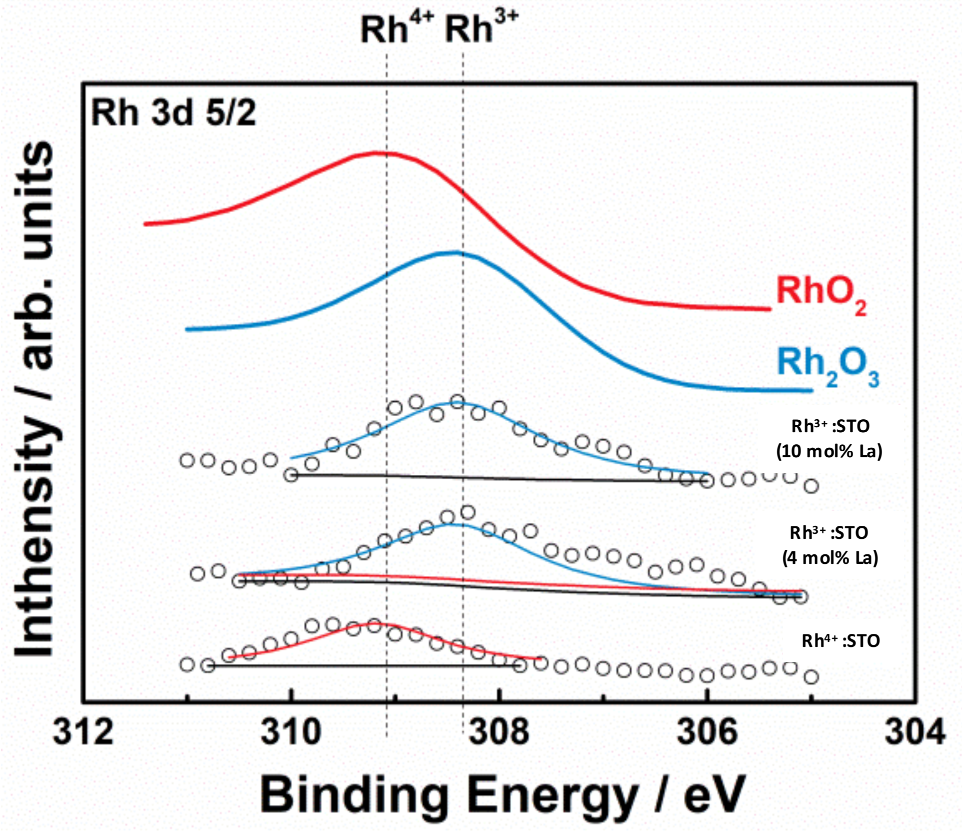

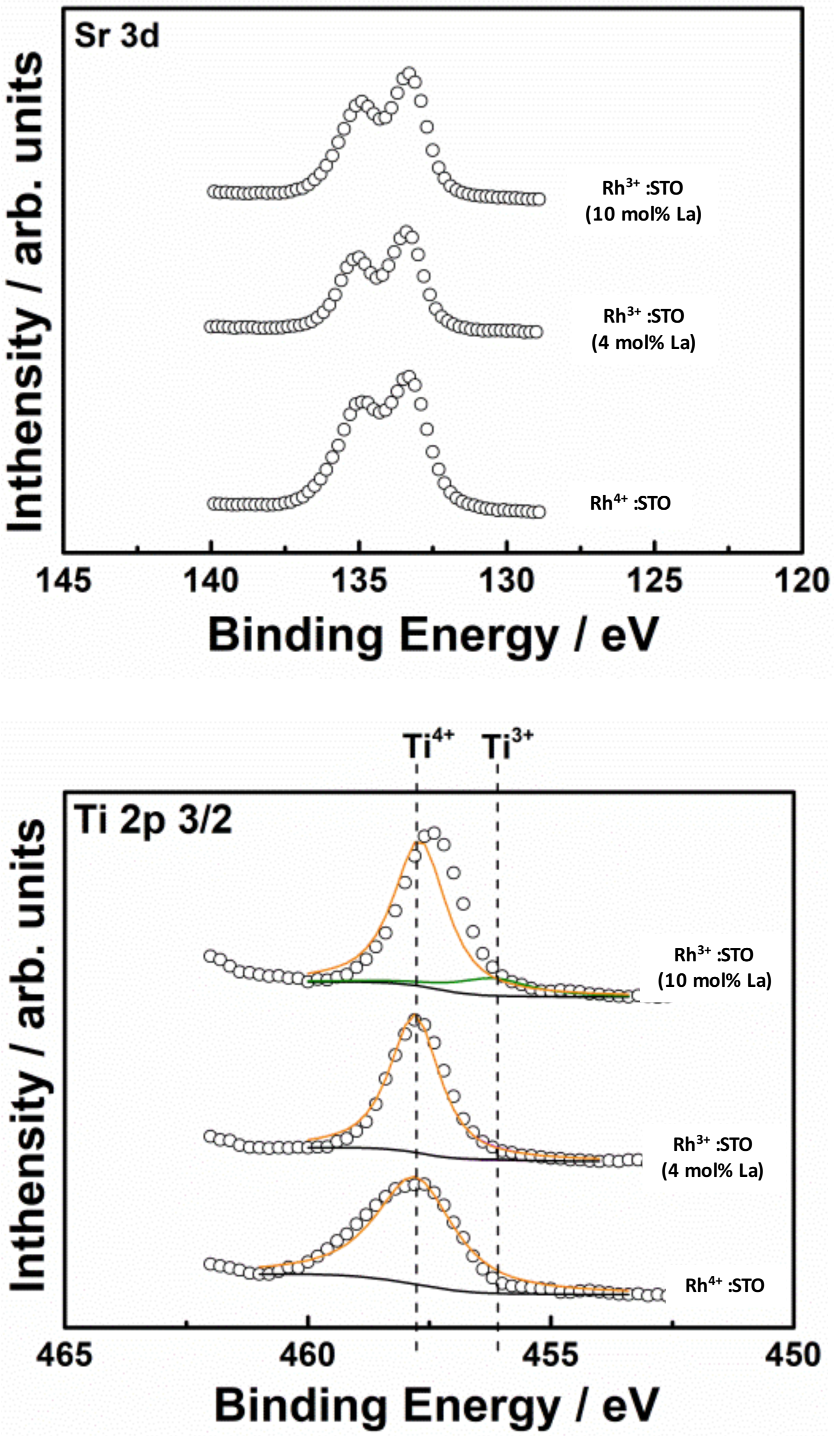

Figure S2. X-ray photoelectron spectra for Rh^{4+}: STO, Rh^{3+}: STO (4 mol% La) and Rh^{3+}: STO (10 mol% La) probing the valence state of Rh, Sr and Ti upon La, Rh doping. Dashed vertical lines are just a guide to the eye. XPS spectra are corrected for instrument broadening by using single crystalline $SrTiO_3$ (111) as a standard. XPS spectra of RhO_2 and Rh_2O_3 are shown for reference corresponding to Rh^{4+} and Rh^{3+} valence states, respectively. In the Rh 3d spectra, red and blue line fits correspond to Rh^{4+} and Rh^{3+}, respectively. In the Ti 2p spectra, brown and green fitted lines correspond to Ti^{4+} and Ti^{3+}, respectively. The black coloured baselines in the Rh 3d and Ti 2p correspond to Shirley XPS baseline.

Table S1. Photocatalytic activities of La, Rh doped $SrTiO_3$ depending on the dopant composition and the doping level.

Sample name	Rh doping level (mol%)	La doping level (mol%)	Valence state of Rh	H_2 evolution rate (micromol/hour)
Rh^{4+}: STO	4	0	Rh^{4+}	24
Rh^{3+}: STO (4 mol% La)	4	4	Rh^{3+}	84
Rh^{3+}: STO (10 mol% La)	4	10	Rh^{3+}	<1

Reaction conditions: catalyst, 0.3 g; cocatalyst, ruthenium, Ru (0.2 wt %); reactant solution, 150 mL of 10 vol % aqueous methanol solution; light source, 300 W xenon lamp ($\lambda > 420$ nm). The valence state of Rh is determined using X-ray photoelectron spectroscopy (XPS).[1]

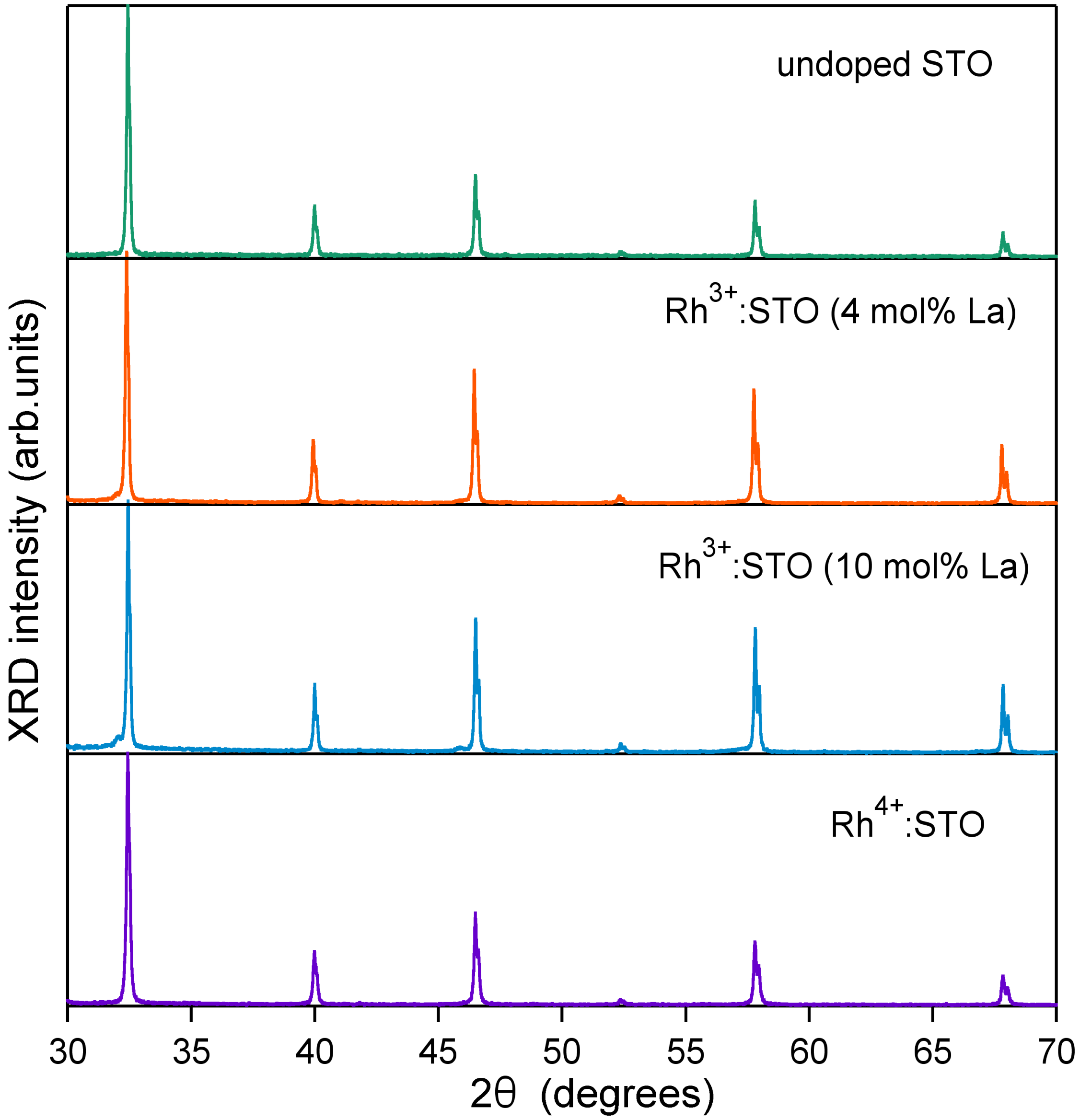

Figure S3. Powder X-ray diffraction patterns for undoped STO, Rh^{3+}: STO (4 mol% La), Rh^{3+}: STO (10 mol% La) and Rh^{4+}: STO.

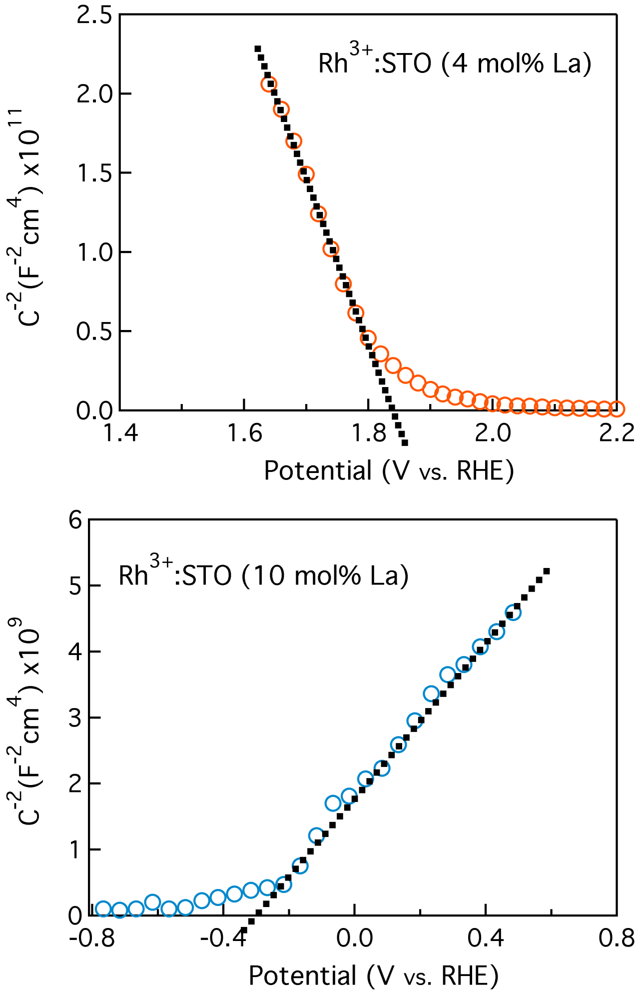

Figure S4. Mott-Schottky plots showing negative and positive slopes for Rh^{3+}: STO (4 mol% La) and Rh^{3+}: STO (10 mol% La) where the intercept with the x-axis shows the flat-band situation.

Note: The Mott-Schottky (M-S) plot is one of the widely-employed methods to determine the flat band potential in photoelectrodes. In the M-S equation, a uniform semiconductor-electrolyte interface is considered while completely neglecting the effect of surface states. In the M-S measurements carried out for 4 mol% and 10 mol% La doped Rh^{3+}: STO, electrodes were fabricated using the particle transfer method where a smooth semiconductor-electrolyte interface is not expected. Despite this inherent limitation, we only use the M-S plot for qualitative determination, i.e., whether the slope is positive or negative using which we can understand whether the semiconductor under study is n- or p-type. As can be observed for Rh^{3+}: STO (4 mol% La), a characteristic negative slope is obtained indicating a p-type behaviour. For Rh^{3+}: STO (10 mol% La), a characteristic positive slope is noticed which is typical of an n-type semiconductor. We tend not to quantitatively determine the precise Fermi level position due to unavoidable errors. Nevertheless, noticing a distinct change in the direction of the slope from negative to positive upon increasing the La doping level indeed supports the transformation of p- to n-type behaviour for Rh^{3+}: STO (4 mol% La) and Rh^{3+}: STO (10 mol% La), respectively.

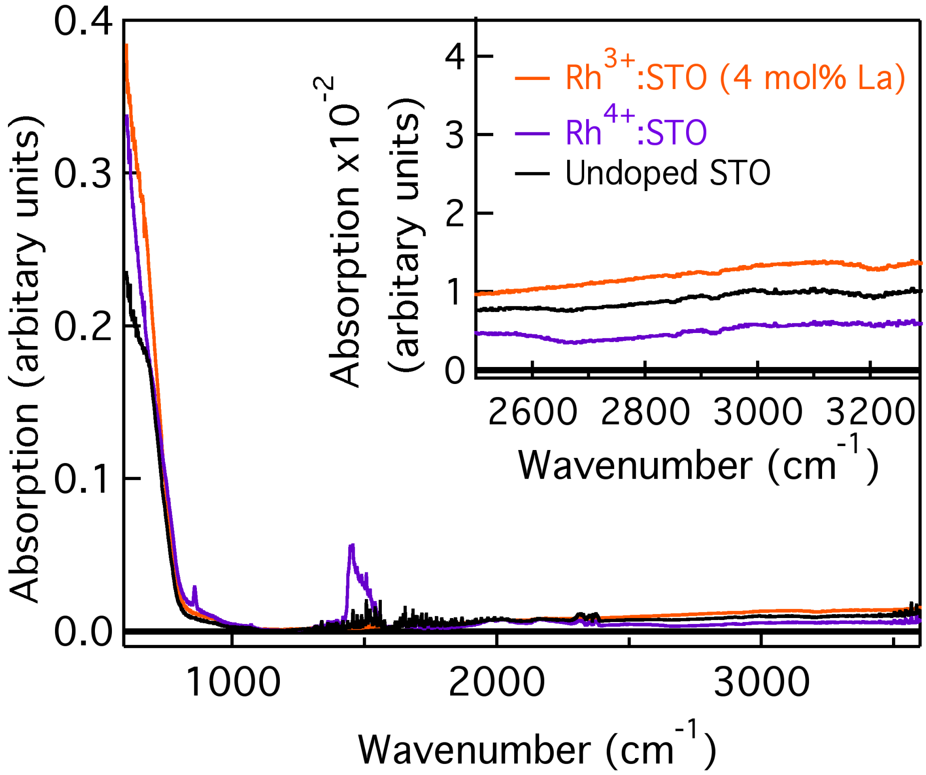

Figure S5. FT-IR spectra recorded for undoped STO, Rh^{3+}: STO (4 mol% La) and Rh^{4+}: STO.

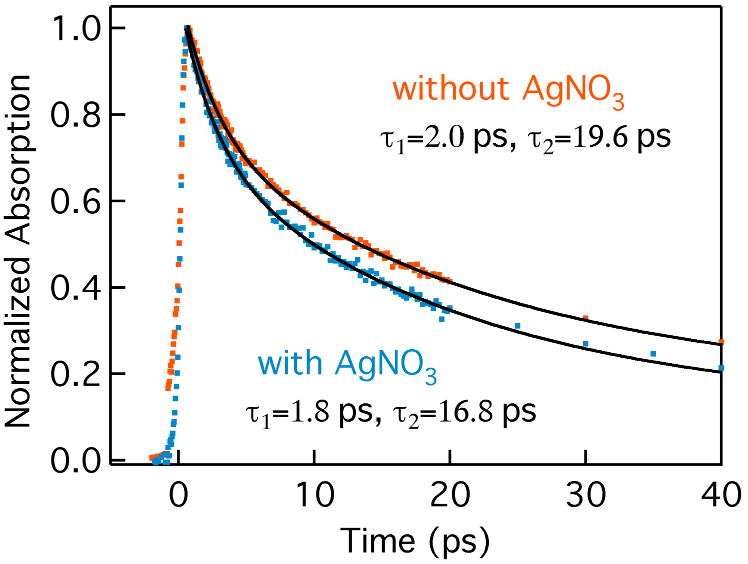

Figure S6. Effect of adding electron scavenger (≈10 μL of 25mM $AgNO_3$ solution to quartz cuvette containing the sample) on the fs-TDR electron decay transients probed at 3435 nm for Rh^{3+}: STO (4 mol% La). Note that both transients are recorded under similar pump fluence (400 nm pump, 2 μJ/pulse) to allow fair comparison. The dark lines are the fits to the transients with a double exponential function.

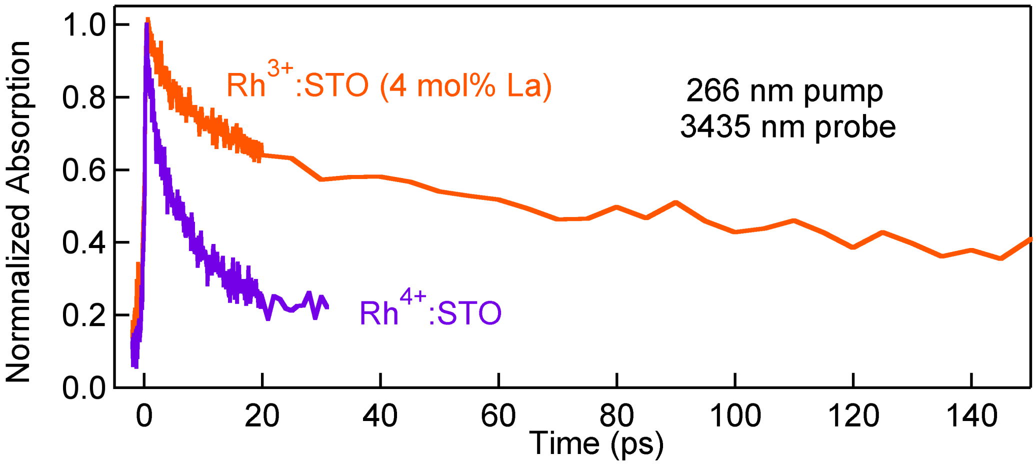

Figure S7. fs-TDR transients for Rh^{3+}: STO (4 mol% La) and Rh^{4+}: STO using 266 nm pump and probed at 3435 nm.

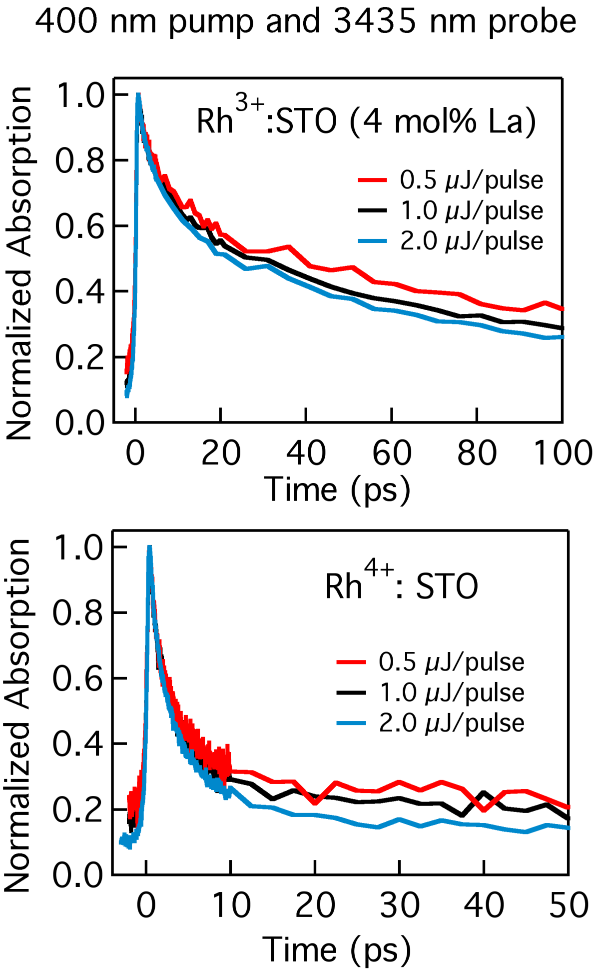

Figure S8. fs-TDR transients corresponding electron dynamics probed at 3435 nm for Rh^{3+}: STO (4 mol% La) and Rh^{4+}: STO using 400 nm pump.

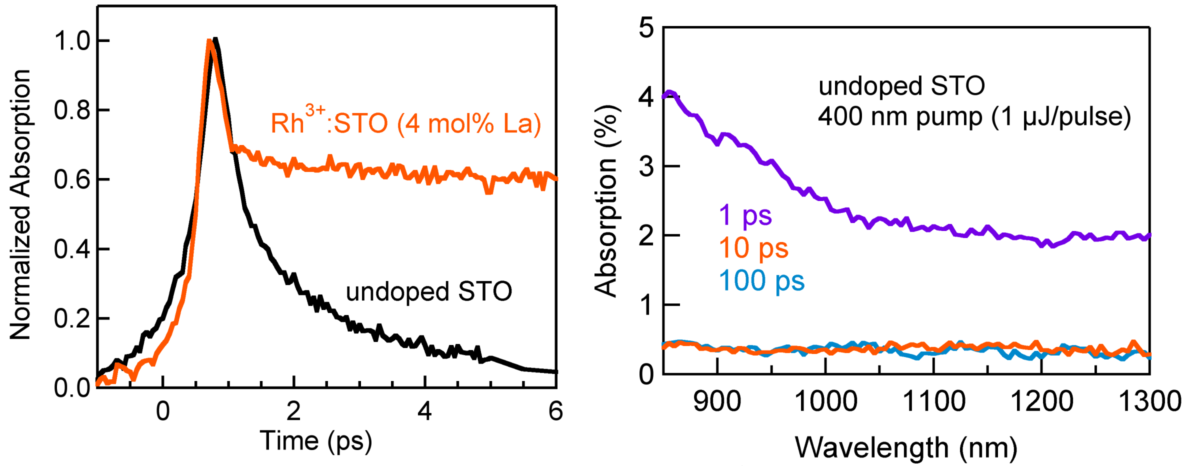

Figure S9. fs-TDR transients for undoped STO and Rh^{3+}: STO (4 mol% La) using 400 nm pump and probed at 920 nm. Right panel show the TA spectra for undoped STO recorded using 400 nm pump with a fluence of 1 μJ/pulse.

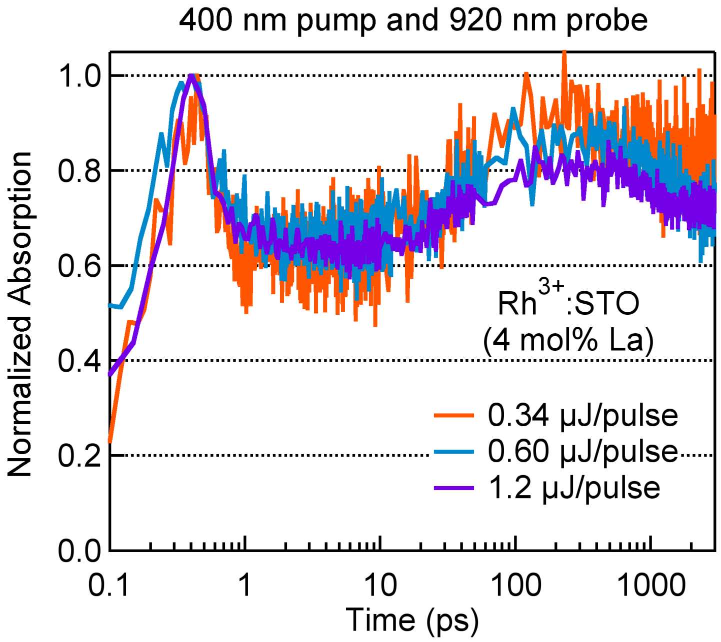

Figure S10. fs-TDR transients recorded at multiple pump fluences for Rh^{3+}: STO (4 mol% La) using 400 nm pump and probed at 920 nm.

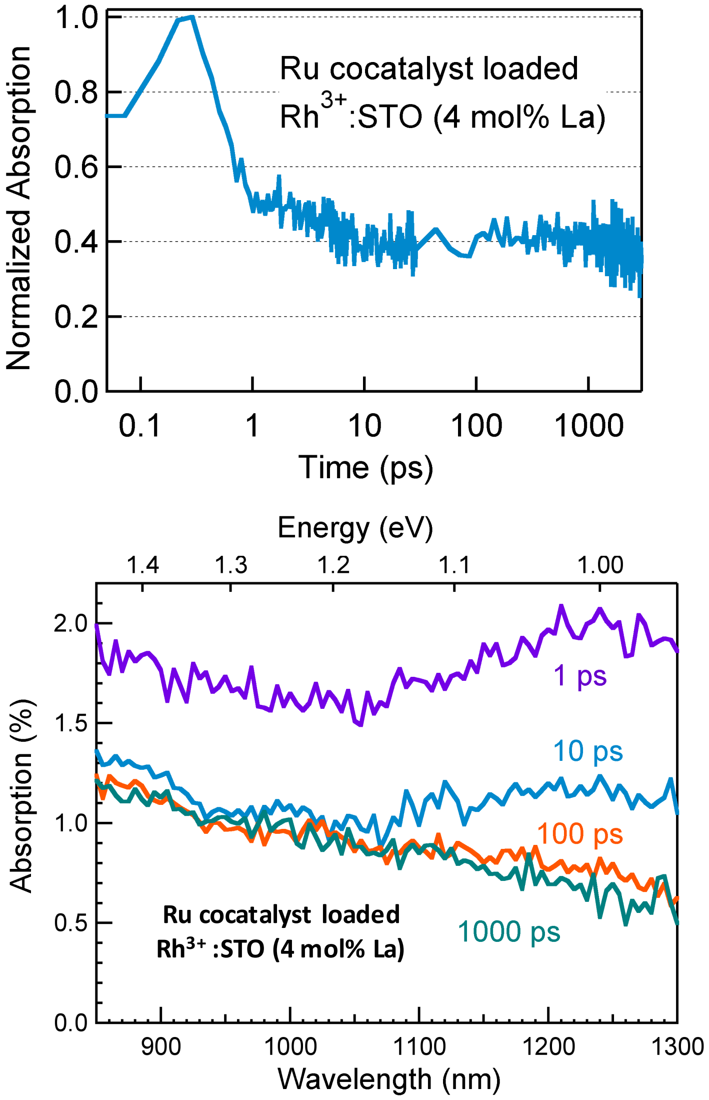

Figure S11. fs-TDR transient for Ru cocatalyst loaded Rh^{3+}: STO (4 mol% La) probed at 920 nm using 400 nm pump with a fluence of 1 μJ/pulse. TA spectra of Ru cocatalyst-loaded Rh^{3+}: STO (4 mol% La) recorded from 850 to 1300 nm using 400 nm pump.

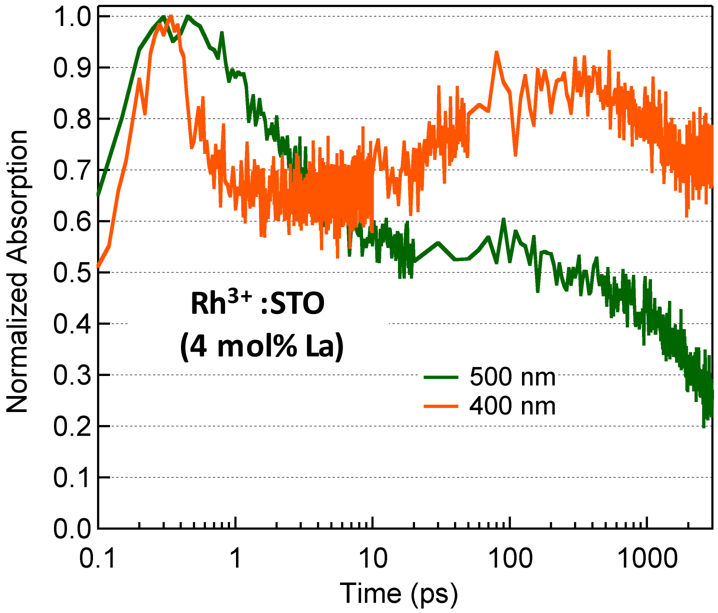

Figure S12. fs-TDR transients for Rh^{3+}: STO (4 mol% La) probed at 920 nm using 400 nm (0.6 μJ/pulse) and 500 nm pump (0.72 μJ/pulse) wavelengths.

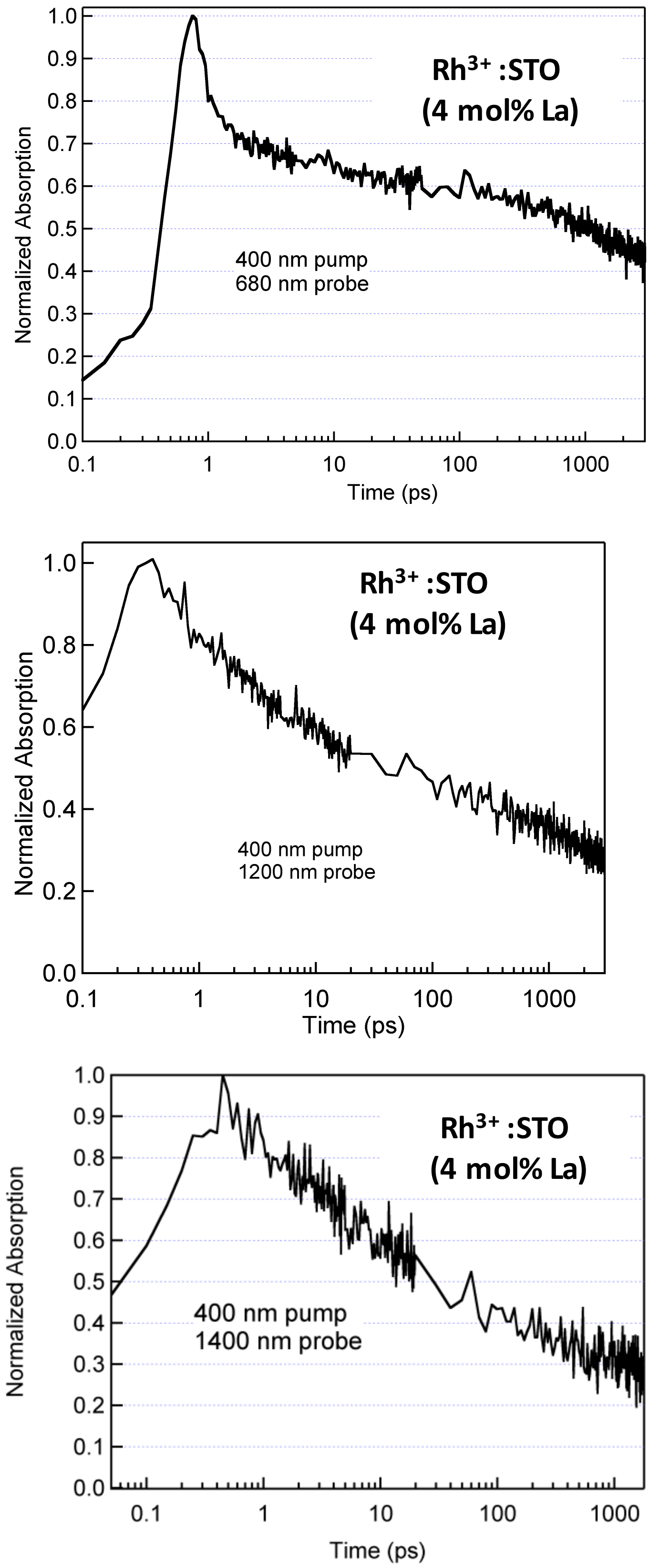

Figure S13. fs-TDR transients for Rh^{3+}: STO (4 mol% La) probed at 680, 1200 and 1400 nm using 400 nm pump. Pump fluence of approximately 0.75 μJ/pulse is employed to conduct all these measurements.

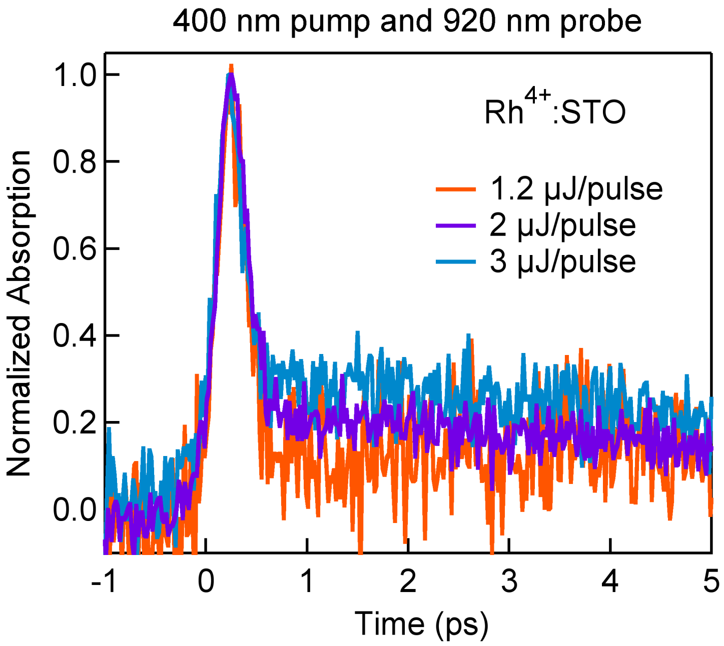

Figure S14. fs-TDR transients recorded at multiple pump fluences for Rh^{4+}: STO using 400 nm pump and at 920 nm probe.

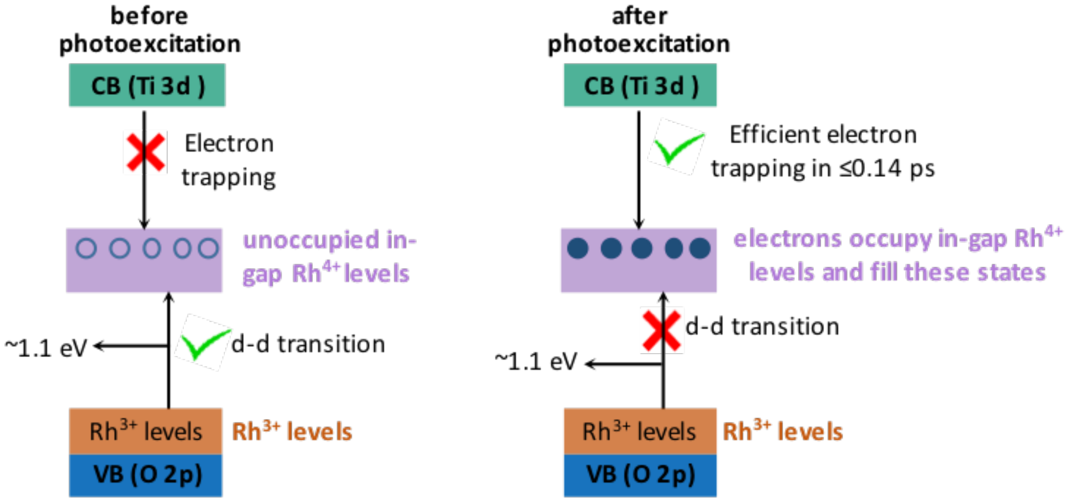

Figure S15. Proposed scheme to explain the bleaching signal noticed at 1010 nm corresponding to d-d transition in Rh^{4+}: STO.

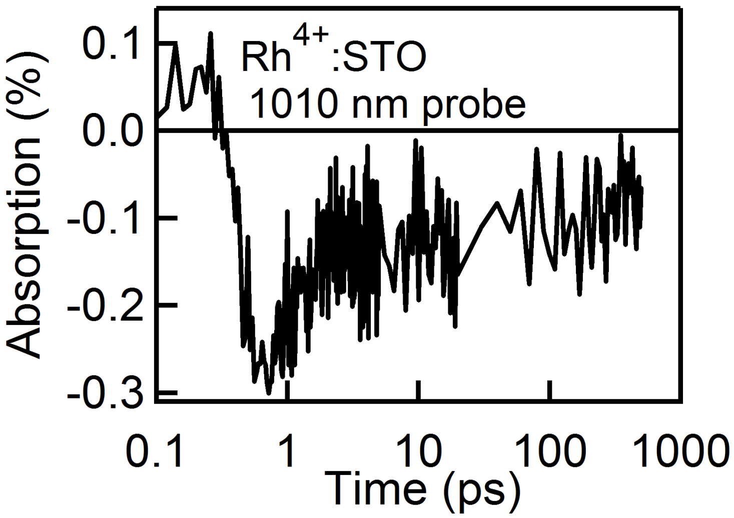

Figure S16. fs-TDR transient for Rh^{4+}: STO probed at 1010 nm using 400 nm pump.

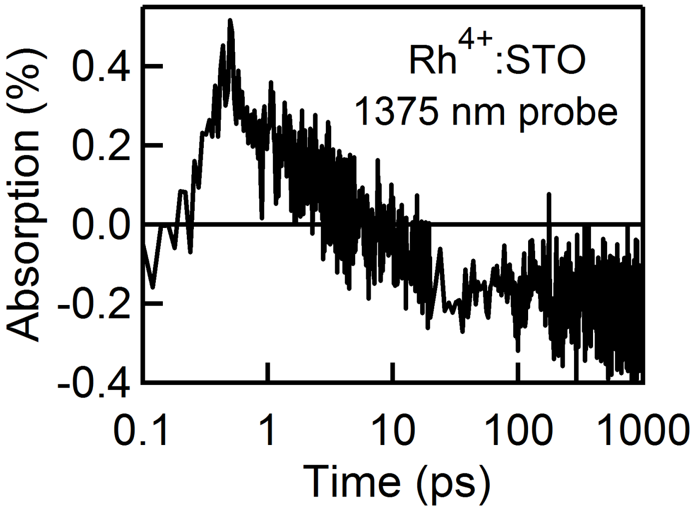

Figure S17. fs-TDR transient for Rh^{4+}: STO probed at 1375 nm using 400 nm pump.

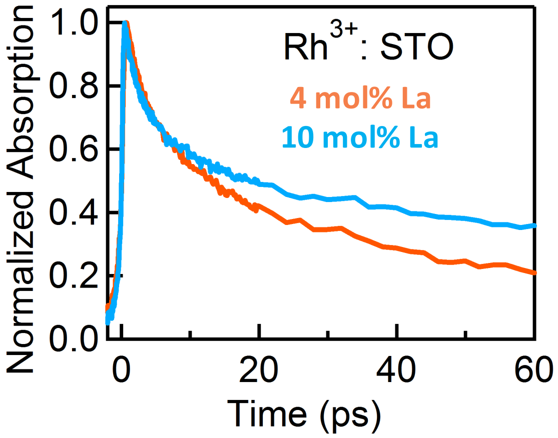

Figure S18. fs-TDR transients corresponding to electron dynamics probed at 3435 nm for Rh^{3+}: STO (4 mol% La) and Rh^{3+}: STO (10 mol% La) using 400 nm pump (2.15 μJ/pulse).

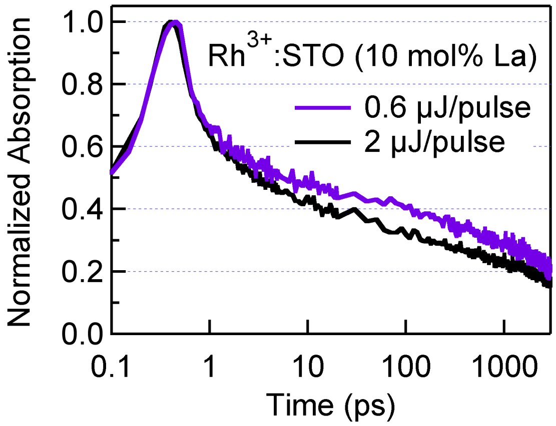

Figure S19. fs-TDR transients probed at 920 nm for Rh^{3+}: STO (10 mol% La) using multiple pump fluences at 400 nm pump.

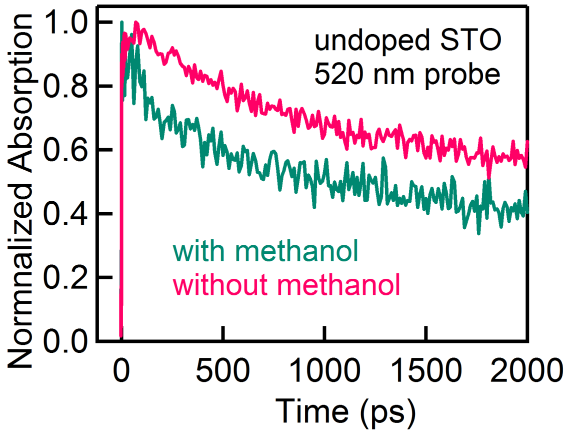

Figure S20. fs-TDR transients for undoped STO (266 nm pump, 520 nm probe) measured with and without hole scavenger (methanol solution) under the similar pump fluence. A faster decay in the presence of methanol indicates that holes are probed at 520 nm.

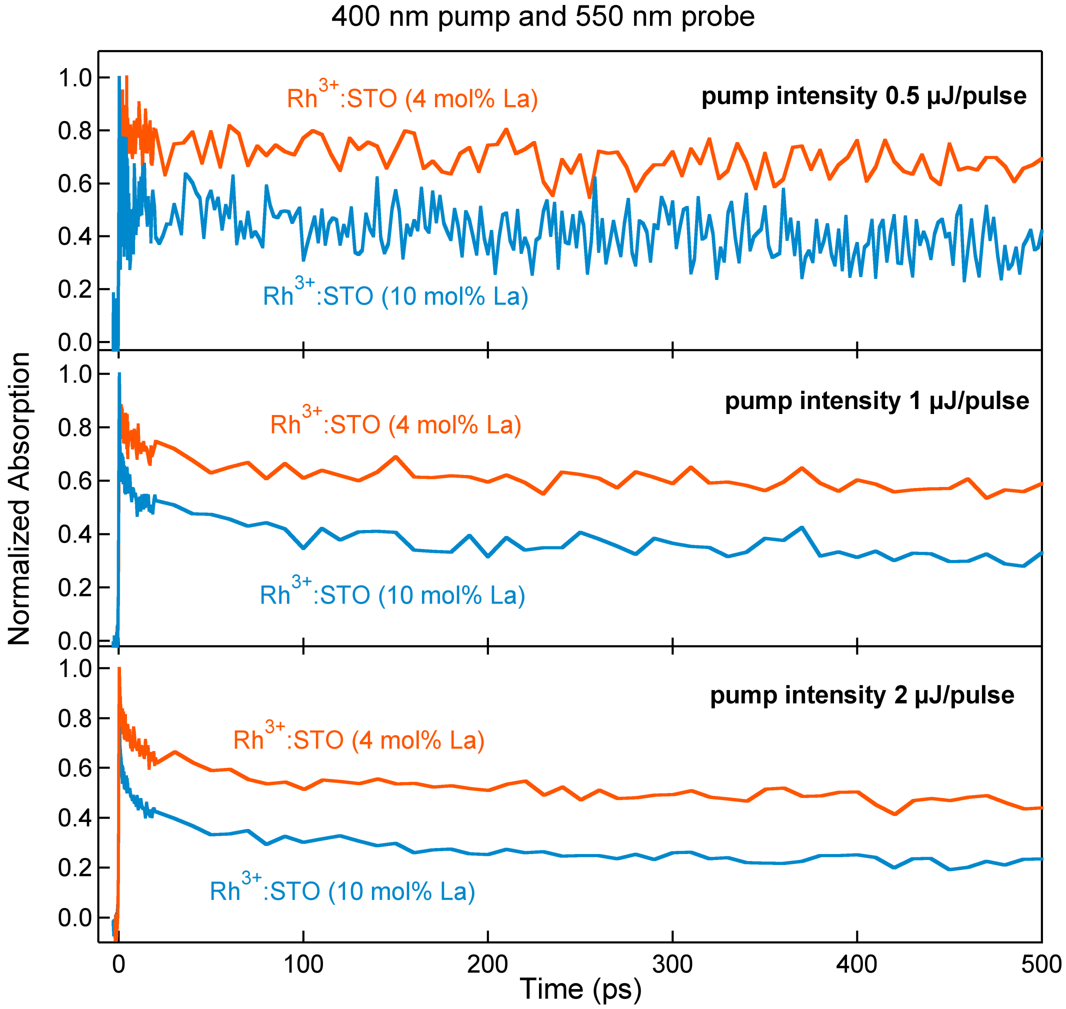

Figure S21. Comparing the effect of pump fluence on the decay of fs-TDR transients probed at 550 nm for Rh^{3+}: STO (4 mol% La) and Rh^{3+}: STO (10 mol% La) using 400 nm pump.

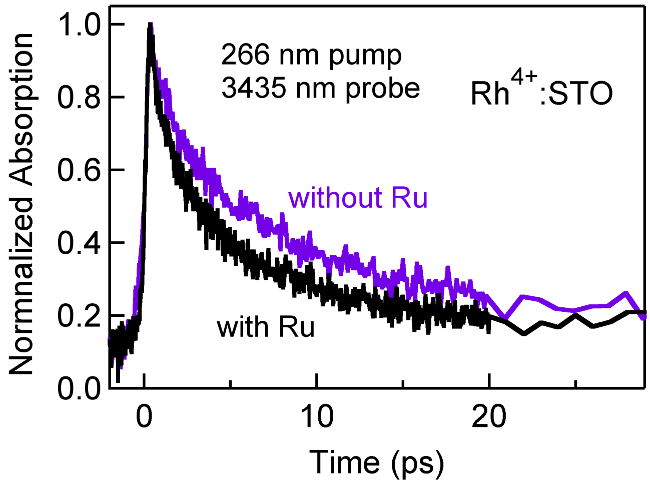

Figure S22. fs-TDR transient for Rh^{4+}: STO with and without cocatalyst loading. 266 nm pump and 3435 nm probe.

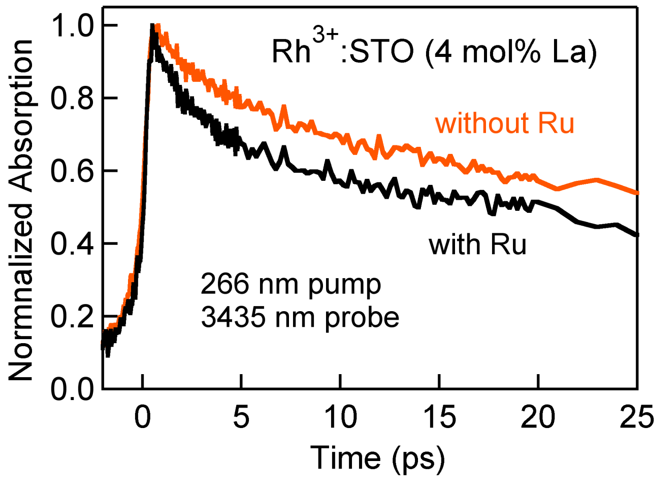

Figure S23. fs-TDR transients for Rh^{3+}: STO (4 mol% La) with and without cocatalyst loading. 266 nm pump and 3435 nm probe.

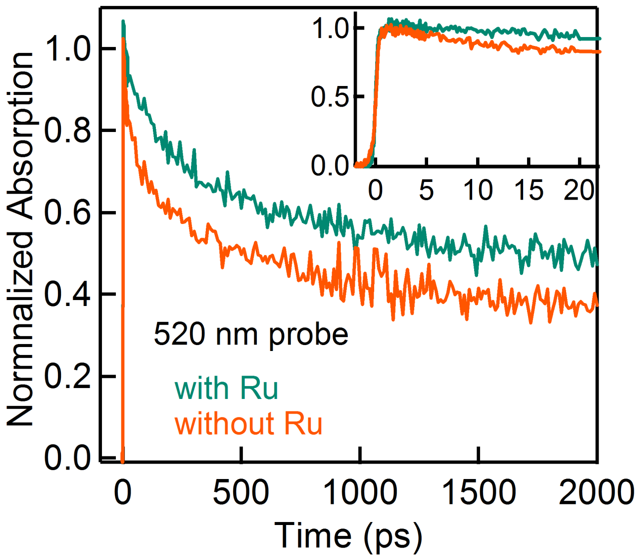

Figure S24. fs-TDR transients for Rh^{3+}: STO (4 mol% La) loaded with and without Ru cocatalyst monitored using 266 nm pump and 520 nm probe.

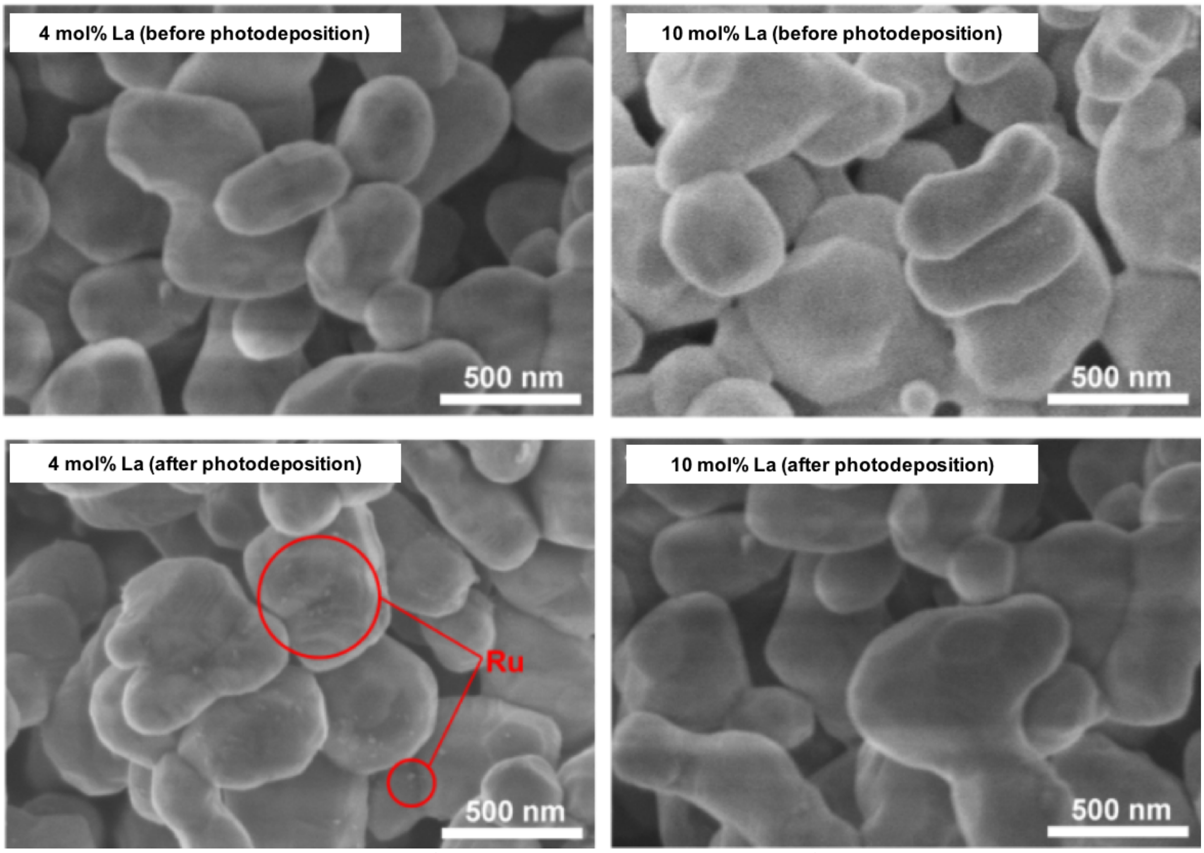

Figure S25. SEM images for Rh^{3+}: STO (4 mol% La) and Rh^{3+}: STO (10 mol% La) before and after photodepositing Ru cocatalyst. However, Ru particles can be barely observed on the surface of Rh^{3+}: STO (10 mol% La).

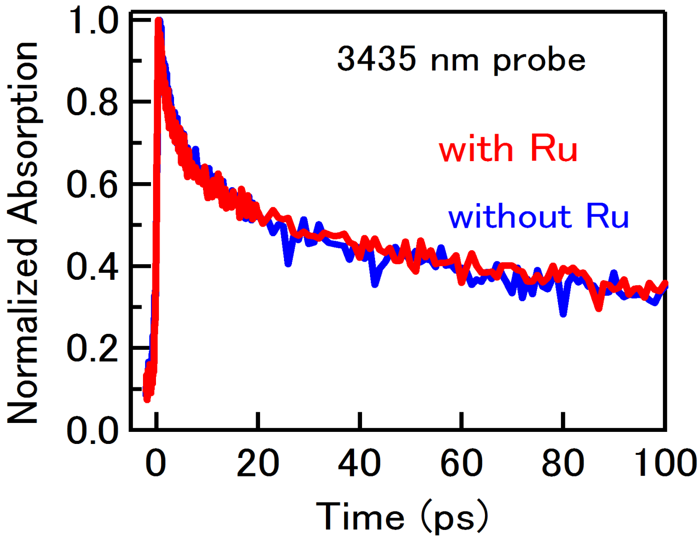

Figure S26. Effect of Ru cocatalyst loading on the dynamics of free electrons for Rh^{3+}: STO (10 mol% La). 400 nm pump and 3435 nm probe is employed.

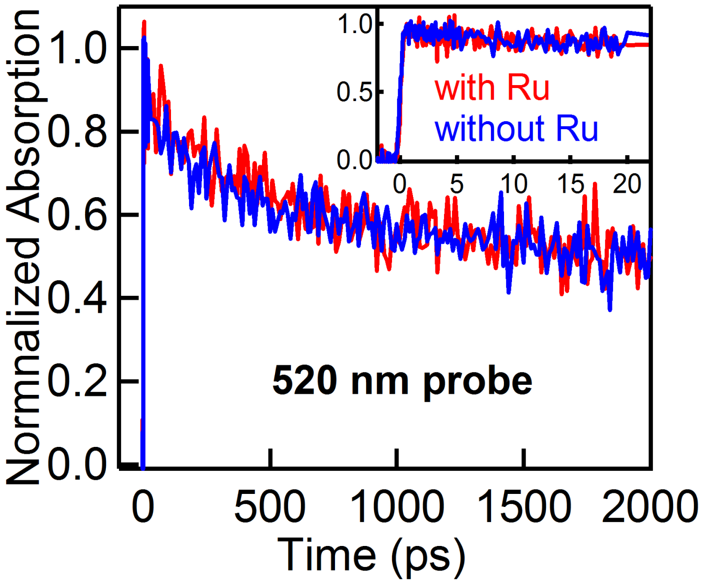

Figure S27. Effect of Ru cocatalyst loading on the dynamics of holes in Rh^{3+}: STO (10 mol% La). 266 nm pump and 520 nm probe is employed.

Appendix 1.

Details regarding the theoretical modeling of the transients to estimate the quantum yield/efficiency and the electron transfer time constant is outlined here.

The concentration of photogenerated electron in the photocatalyst with and without Ru cocatalyst loading at time *t* is denoted as $\rho_{Ru}(t)$ and $\rho(t)$, respectively. Both $\rho(t)$ and $\rho_{Ru}(t)$ are normalized by the values at *t=0*, so that the normalized concentration can be interpreted as the survival probability of carriers probed at 3435 nm. We assume that the electron concentration in the photocatalyst decay homogeneously in space in the absence of Ru cocatalyst. However, in the presence of Ru cocatalyst, a part of the electrons may reach Ru. The fraction of electrons that can be transferred to Ru is denoted as *f*. The other part of electrons is assumed not to be influenced by Ru cocatalyst. This assumption is logical considering the fact that Ru cocatalyst loading is 0.2 wt% and the surface of the photocatalyst is not completely covered with Ru.

When the electron transfer from the photocatalyst to the Ru cocatalyst competes with the other relaxation processes (for e.g., trapping), we relate the parameters *f*, $\rho(t)$ and $\rho_{Ru}(t)$ by, $\rho_{\mathrm{Ru}}(t)=\rho(t)\left(f\exp(-k_{\mathrm{et}}t)+1-f\right)$, (1)

where k_{et} is the electron transfer rate.

The efficiency of electron transfer can be obtained from

$$\int_0^\infty dt k_{\mathrm{et}} f\rho(t)\exp(-k_{\mathrm{et}}t)\,, \tag{2}$$

where the integrand represents the fraction of electrons transferred to the Ru per unit time eventually allowing us to calculate the efficiency of electron transfer to Ru.

Below, we apply Eq. (1) to estimate the electron transfer rate from the experimental data of Figure 7 of the main text. In order to estimate the k_{et}, the decay of electrons in the photocatalyst without Ru is assumed to be expressed by the following function (double exponential decay terms plus a constant term),

$$\rho(t) = y_0 + \sum_{j=1}^{2} A_j \exp\left(-t/\tau_j\right), \tag{3}$$

where τ_j is the decay time. The τ_j values for Rh^{4+}: STO are found to be τ_1= 1.14 ps and τ_2 = 5.96 ps. While the τ_j values for Rh^{3+}: STO (4 mol% La) are found to be τ_1= 2.0 ps and τ_2 =19.9 ps.

Using the Eq. (1) and the Eq. (3), we can theoretically obtain the electron concentration in the photocatalyst, where *f* and k_{et} are the fitting parameters. The *f* values for Rh^{3+}: STO (4 mol% La) and Rh^{4+}: STO are 0.16 and 0.12, respectively. We accounted for the possible ultrafast electron transfer by convoluting the transients with the instrumental response function approximated by a Gaussian function with the full width at half maximum (FWHM) of 0.141 ps. By fitting the theoretical relation to the corresponding data, the time constant for electron transfer, ($1/k_{\mathrm{et}}$) was found to be 1.6 ps and around 0.29 ps for Rh^{3+}: STO (4 mol% La) and Rh^{4+}: STO, respectively.

The quantum yield/efficiency of electron transfer from Rh^{3+}: STO (4 mol% La) to the Ru cocatalyst is found to be 14.7%. We used similar approach to determine the quantum yield of electron transfer from Rh^{4+}: STO to the Ru cocatalyst. However, the fit from the model deviates with the experimentally obtained transient in the early 0.5 ps and after 4 ps. Hence, we could not precisely determine this value.

Reference:

1. Q. Wang, T. Hisatomi, S. S. K. Ma, Y. B. Li and K. Domen, *Chem. Mater.*, 2014, **26**, 4144-4150.